An archaeal CBASS system eliminates viruses without killing the host cells

Deepak Kumar Choudhary, Himani Singla, Dana Vassover, Noam Golan, Leah Reshef, Hadar Shukrun, and Uri Gophna

The Shmunis School of Biomedicine and Cancer Research, George S. Wise Faculty of Life Sciences, Tel Aviv University, Tel Aviv, Israel

Correspondence to: urigo@tauex.tau.ac.il

Abstract

Many CBASS systems defend against viral infections by depleting cellular NAD+ levels, eventually leading to dormancy or death. This abortive infection strategy is beneficial in stopping fast lytic infections, as cells die before spreading the virus to neighboring cells. However, in co- chronic viral infections, which often occur in archaea, abortive infection could be detrimental, as the cost of immunity may outweigh that of infection. Here we study an archaeal CBASS system that was expressed in the model organism *Haloferax volcanii* DS2. We demonstrate that this system protects against a chronically infecting virus, HFPV-1, and eliminates the virus after several passages without killing the host. Moreover, cells that cleared the virus became substantially more resistant to subsequent HFPV-1 infections. Cell death only occurred after extensive incubation with HFPV-1. These findings suggest that CBASS can be beneficial during non-lytic infection, potentially explaining why such systems are common in archaea.

Introduction

The cyclic-oligonucleotide-based antiphage signalling system (CBASS) protects bacterial populations by killing the cell before the phage reaches maturation by diverse mechanisms, thereby stopping infection spread [1–6]. These systems share a common ancestry with the cyclic GMP–AMP synthase (cGAS)–STING immune pathway of animals[1,7–9] , and act by sensing a viral infection and producing a cyclic-oligonucleotide signal molecule, which is then sensed by an effector protein that later causes cell death. CBASS is fairly common and present in over 10% of bacterial genomes and in many archaeal genomes [1,5,10]. One of the most common effector types in CBASS is a TIR-SAVED domain protein that upon sensing the signal molecule depletes cellular NAD^+ levels, resulting in cell death[11,12].

Abortive-infection systems, such as CBASS, are beneficial in stopping a rapid lytic infection because cells die before spreading the virus to closely-related sister cells. Importantly, cells at advanced stages of lytic infection have nothing to lose from suicide, since they will soon lyse anyway when the phage completes its lifecycle. Conversely, many archaea, in their natural habitats, are infected by non-lytic viruses that chronically co-exist with their hosts for extended

35 periods. Under such situations, abortive infection should in principle be harmful because the
36 cost of immunity may be higher than that of infection, yet intriguingly CBASS is about as
37 common in archaea as they are in bacteria.

38 Here we heterologously expressed an archaeal Type II CBASS system from *Haloferax* strain
39 Atlit 48N (H-CBASS2, see below), in the model organism *Haloferax volcanii* and tested its
40 activity during chronic infection by the model virus HFPV-1. We show that the CBASS system
41 is beneficial in this non-lytic infection model, and enables clearing of that virus after several
42 passages, without killing the host. Surprisingly, cells that cleared the infection become faster-
43 growing compared to their parental genotype prior to infection, or to uninfected H-CBASS2-
44 negative controls. This suggests that CBASS systems might provide benefits to archaea
45 dealing with persistent viral infections, which could account for their widespread presence in
46 these organisms.

47 **Results and discussion**

48 ***Expression of type II CBASS in H. volcanii leads to growth delay during virus infection,***
49 ***in a cyclase-dependent manner***

50 *Haloferax* strain 48N encodes two CBASS gene clusters and is also chronically infected by
51 two viruses, making it sub-optimal for characterization of individual defense systems. We
52 therefore opted for using the model haloarchaeal strain *H. volcanii* DS2 as a heterologous
53 host instead. We cloned the *Haloferax* 48N CBASS Type II system (H-CBASS2 for short) into
54 the high-copy replicating plasmid pTA927, which contains an inducible promoter, and
55 transformed it into *H. volcanii* which does not encode any CBASS naturally (Fig. 1A). We
56 examined the growth profile of the transformed cells and observed a small degree of growth
57 inhibition upon H-CBASS2 expression in *H. volcanii*, in comparison to a negative control strain
58 containing an empty pTA927, indicating small but noticeable toxicity (Fig. 1B). Next, we
59 wanted to assess if H-CBASS2 mediated an anti-viral response during infection. Since there
60 are no known lytic viruses available for *H. volcanii*, we used the model virus HFPV-1 that
61 causes a chronic non-lytic infection [13]. This also has the advantage of testing whether CBASS
62 is beneficial or detrimental during an a relatively mild chronic infection. We started from virus-
63 infected colonies (see Methods) and used tryptophan induction to test for the activity of the
64 system. Notably, virus infected cells that were induced to express H-CBASS2 showed
65 substantial growth inhibition compared to non-infected cells, or to HFPV-1-infected cells
66 carrying an empty vector (Fig, 1C). These results suggest that the Type II CBASS system from
67 48N is active in *H. volcanii* and responds to viral infection.

68 A BLASTP analysis revealed that the H-CBASS2 cyclase had 42% sequence identity with the
69 *Enterobacter cloacae* CBASS CDnD cyclase (Extended Fig. 1), which is known to produce

cyclic AMP-AMP-GMP upon viral infection[14]. Additionally, we created a homology model of the H-CBASS2 cyclase using AlphaFold3, confirming that the aligned region has about 40% sequence identity and a TM-score of 0.8259 with the *E. cloacae* cyclase Fig. 1D). We could therefore identify the active site tyrosine at position 237 in the H-CBASS2 cyclase and mutate it to alanine. This mutation was shown in the *E. cloacae* cyclase to completely abolish c-AAG synthesis, emphasizing the essential role of this residue in the cyclase activity [14]. Indeed, the Y237A mutation in the H-CBASS2 cyclase rescued the substantial growth inhibition caused by viral infection in the presence of H-CBASS2, as well as the minimal growth inhibition caused by H-CBASS2 alone (Fig. 1E). This suggests that the H-CBASS2 cyclase, similar to *E. cloacae* CDnD, produces a signalling molecule in response to viral infection that is critical for activity.

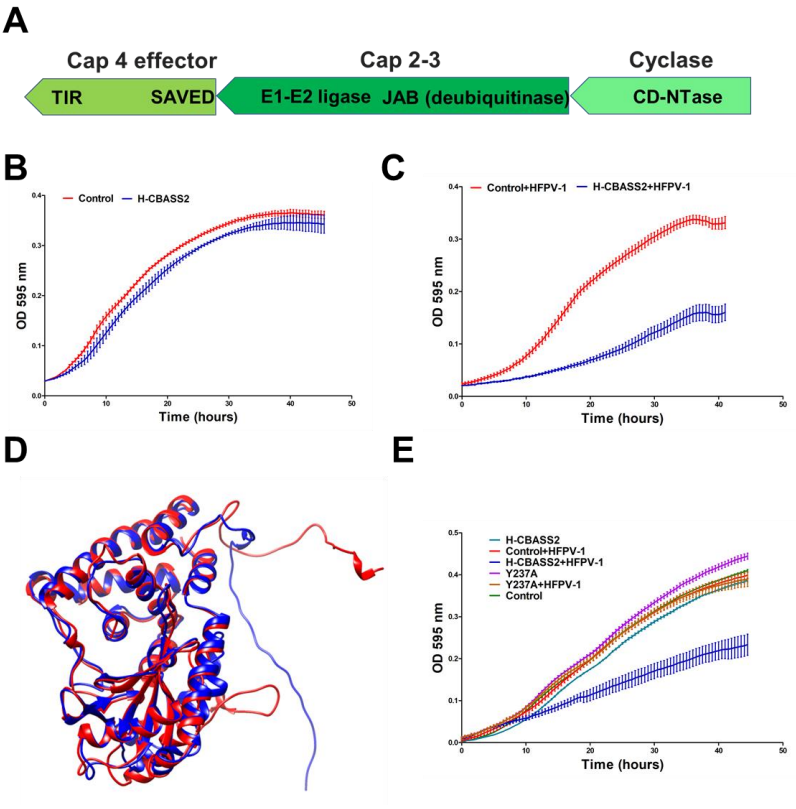

Figure 1. HFPV-1 infection causes growth delay in H-CBASS2 expressing cells. A) The *Haloferax* 48N-CBASS Type II operon. H-CBASS2 genes were cloned into the pTA927 plasmid, under the inducible tryptophanase promoter and transformed into *H. volcanii* WR540. **B)** Growth curves of *H. volcanii* expressing H-CBASS2 under tryptophan inducible promoter (blue) and control (with empty vector) (red), without viral infection. **C)** HFPV-1 particles were transformed into H-CBASS2-expressing *H. volcanii* cells, and then virus-infected colonies were selected by screening with PCR. Growth curves of virus-infected H-CBASS2-expressing *H. volcanii* (blue) under tryptophan inducible promoter and infected control (red) are shown. **D)** 3D structural alignment of the predicted H-CBASS2 cyclase (Alphafold 3) structure aligned with the crystal structure of the *E. cloacae* cyclase using Foldseek (TM score-0.82595 and RMSD of 7.3). **E)** Growth curves of mutated H-CBASS2 cyclase with or without virus infection. Y237A mutation on the H-CBASS2 cyclase without infection (purple) and with infection (brown), control

without infection (green) and with infection (red), wild-type H-CBASS2 without infection (cyan) and with infection (blue). B, C and E: Lines represent the mean of at least 3 biological replicates, each with three technical replicates.

H-CBASS2 does not lead to immediate cell death upon HFPV-1 infection

CBASS systems are considered to be abortive infection systems that kill the cell in order to stop viruses from spreading to neighbouring sister cells. Specifically, a bacterial type II CBASS system has been shown to deplete cellular NAD^+ levels and bring about cell death[11]. We therefore performed live-dead staining assays on logarithmic cultures of HFPV-1-infected cells expressing H-CBASS2. Surprisingly, we detected very few dead cells, and their ratio in the culture did not exceed that observed in the vector-only control (Fig. 2A). Given that H-CBASS2 does not cause abortive infection, we therefore wondered whether it could nonetheless stop or delay the spread of HFPV-1 infection. HFPV-1 is a virus that does not lyse host cells and does not form plaques using standard approaches [13]. However, since this virus does delay host growth, we used a recently developed protocol that enables the detection of plaques produced by non-lytic viruses of haloarchaea[15]. These plaques are caused by growth inhibition, as is commonly observed upon infection with non-lytic phages, such as M13 [16]. Surprisingly, expression of H-CBASS2 did not substantially reduce the plaquing efficiency of HFPV-1 (Fig. 2B). Thus, H-CBASS2 probably cannot interfere with the early stages of infection by HFPV-1.

Long-term exposure to viral infection in HCBASS-2-expressing cells reduces viability

Although we did not detect any short-term cell mortality, we did observe that virus-infected H-CBASS2-expressing colonies left at room temperature for 4-5 weeks became bleached (Fig. 2C, see also time series in Extended Fig. 2), losing the pink-red pigmentation typical of Haloferax cells that naturally synthesize the carotenoid pigment bacterioruberin[17,18] . When suspending cells from the bleached colonies and submitting them to Live-Dead assays, we observed that many of the cells from those colonies were dead. In contrast, 4–5-week-old colonies of infected cells that did not express H-CBASS2 maintained normal color and viability (Fig. 2D). Importantly, carotenoids as well as essential archaeal membrane lipids both share a key building block, mevalonate, synthesized from HMG-CoA by the enzyme HMG-CoA reductase that uses two molecules of NADPH[19] . Thus, it is likely that the depletion of cellular NAD (and NADPH) will force cells to scavenge mevalonate from carotenoids into the more critical membrane lipids, resulting in the observed bleached phenotype.

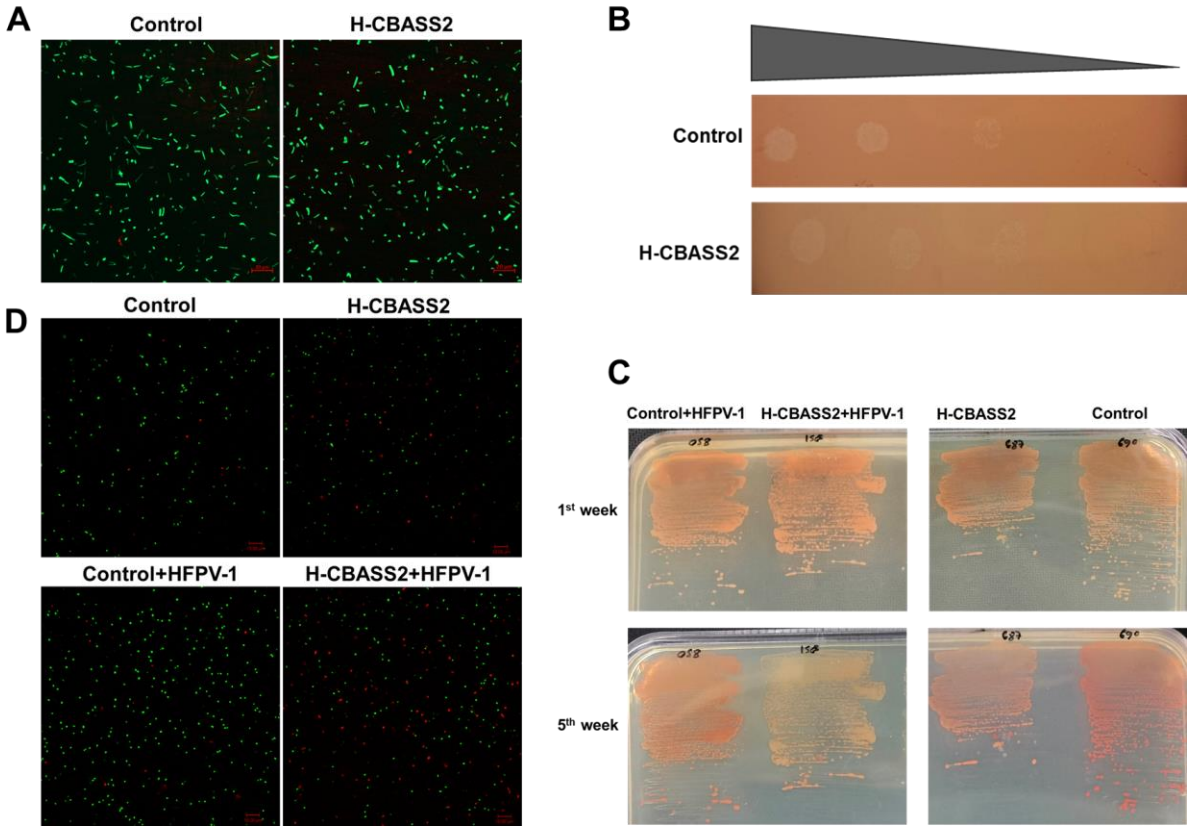

Figure 2. H-CBASS2 does not cause rapid cell death Upon HFPV-1 infection A) Representative confocal microscopy images depicting Live/Dead assays of log. -phase cells. H-CBASS2-expressing cells and control cells with an empty vector, both infected with HFPV-1 (Scale bar: 20 µm). Data are representative of at least 3 independent experiments. **B)** Plaque assay using 10-fold serial dilutions of virus (left-most is a 10^{-4} virus dilution suspension). H-CBASS2 expressing cells and control cells with an empty vector were mixed with 0.02% top agar and plated onto rich medium. Afterward, 3 µL of serial dilutions of HFPV-1 were spotted to quantify plaquing efficiency. The images are representative of at least three biological replicates. **C)** Representative images of colony colour of *H. volcanii* cells infected with HFPV-1. A plate streaking assay was performed using *H. volcanii* strains expressing H-CBASS-2, with and without virus infection, along with a control containing an empty vector. A 20 µl log. -phase culture was streaked onto fresh plates, which were incubated at 45°C for 4-5 days. After growth became visible, the plates were kept at room temperature for 4-6 weeks, with images taken every 3 days. Virus-infected H-CBASS2-expressing colonies left at room temperature for 4-6 weeks showed obvious bleaching**. D)** Live/Dead assays conducted on cells from bleached colonies, revealing a higher number of dead cells in the virus-infected *H. volcanii* strain with H-CBASS-2 compared to the control (Scale bar: 10 µm).

HCBASS-2-expressing cells require long-term exposure to viruses for NAD depletion

H-CBASS2 has the same architecture as many bacterial type 2 CBASS systems, with effector proteins comprised of a SAVED domain and a TIR domain. In such systems, the SAVED domain senses the cyclic-oligonucleotide signal molecule, while the TIR domain has been shown to be the effector domain and cause cell death by depletion of NAD^+ [11]. H-CBASS2 is therefore expected to function via NAD^+ depletion. We therefore quantified total NAD levels during HFPV-1 infection of cells expressing H-CBASS2 (see Methods). Notably, total NAD

levels were largely unaffected in infected H-CBASS2-expressing cells during logarithmic growth compared to controls with an empty vector (Fig. 3A). In contrast, duringlate logarithmic phase, we observed a slight reduction in NAD levels in the H-CBASS2-expressing cells (Fig. 3A). Furthermore, when we measured NAD levels from the bleached colonies described above (Fig. 3B), we observed that NAD levels were greatly decreased in virus-infected *H. volcanii* with CBASS compared to infected cells with the empty vector. We also observed a substantial decrease in NAD levels in H-CBASS2-expressing cells from 4-week-old colonies that were not infected. These results suggest that NAD depletion in *H. volcanii* cells by H-CBASS2 upon chronic viral infection is a slow process and becomes lethal only after many generations of growth. This is reminiscent of type III CRISPR-Cas systems that cause dormancy at first, "buying time" for additional defense systems to destroy the virus, and only subsequently resulting in cell death[20–22].

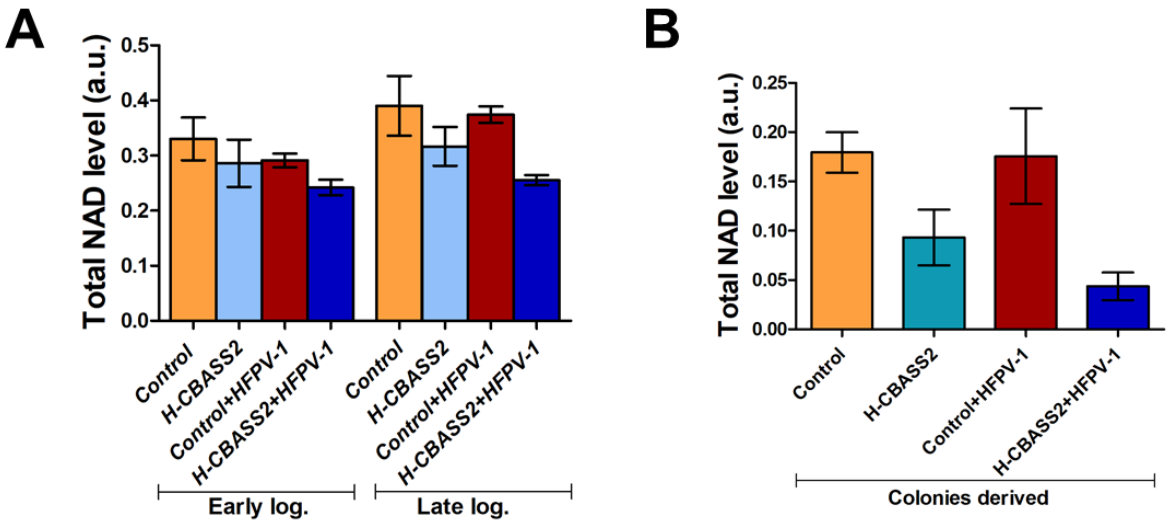

Figure 3. NAD levels in HCBASS-2-expressing cells only decrease after sustained virus exposure. A) NAD levels in *H. volcanii* strains expressing H-CBASS-2, in the presence or absence of virus infection. Strains were grown to early-log. and late log. growth phases. Equal numbers of cells from each culture were collected and total NAD levels were measured using the NAD/NADH Quantification Kit. Data are representative of at least three independent experiments. **B)** NAD levels in cells from bleached colonies. After resuspending the bleached cells (which had been incubated for 4-5 weeks) in fresh medium, protein concentration of the biomass was determined using the Bradford method. A biomass with equal protein concentration from each strain was then used to measure total NAD levels. Data are representative of at least three independent experiments.

H-CBASS2 eradicate HFPV-1 infection

Since HFPV-1 infection is relatively mild while H-CBASS2 activity can be harmful and even lethal, the question arises whether such a system benefits the host during chronic infection, or whether it is deleterious. Accordingly, we performed a head-to-head competition experiment

171 in which we grew together HFPV-1-infected *H. volcanii* cells, with or without H-CBASS2. As
172 expected, at 24 and 48 hours after mixing, the H-CBASS2-negative cells increased in relative
173 abundance at the expense of the H-CBASS2-positive cells (Fig. 4A), indicating that in the
174 short-term H-CBASS2 is detrimental during infection.

175 If H-CBASS2 is deleterious during infection with a chronic virus, prolonged growth of H-
176 CBASS2-expressing cells infected with a virus should select for cells in which the system
177 became inactivated by mutation. Alternatively, the cells will try to eliminate the virus, and if
178 successful, one may conclude that the system is beneficial. In order to test these competing
179 scenarios, we performed an in-vitro evolution experiment where we grew HFPV-1-infected *H.*
180 *volcanii* cells with and without H-CBASS2 separately in liquid culture until the late stationary
181 phase, and then used that culture to inoculate fresh medium and repeated this for ~10
182 passages, taking samples at passages 3, 6, and 10 (Fig. 4B). We then plated the diluted
183 cultures from these time points on solid media and screened 30-40 colonies for the presence
184 of HFPV-1 (Extended Fig. 3a and 3b for PCR screen gels). Remarkably, nearly all colonies
185 from H-CBASS2-expressing cells no longer had detectable virus DNA at passage 10, in all
186 three biological replicates, while over 95% of colonies that did not express H-CBASS2 still had
187 viral DNA presence (Fig. 4C, 3D, 3E). Even as early as passage 3 (about 80 generations),
188 most H-CBASS2-expressing colonies did not have detectable viral DNA. In comparison, the
189 presence of the H-CBASS2 insert was confirmed by PCR after the 10th passage in all colonies
190 from the H-CBASS2-expressing culture (Extended Fig. 3c). Notably, we sequenced several
191 colonies after passage 10th and did not observe any mutation in the H-CBASS2 or the vector
192 that harbors it.

193 We then performed qPCR to quantify the level of virus DNA in the supernatant after 48 and 72
194 hours of growth and observed almost a 20% decrease in viral DNA in the supernatant in the
195 CBASS-expressing cells compared to the control cells. Moreover, we also observed 20%
196 lower levels of viral DNA after the 4th passage and 40% lower levels of viral DNA after the 6th
197 passage in the CBASS-expressing cells, which can probably be attributed to virus clearing in
198 the majority of cells at these later stages (Extended Fig. 4a, b, c, and d).

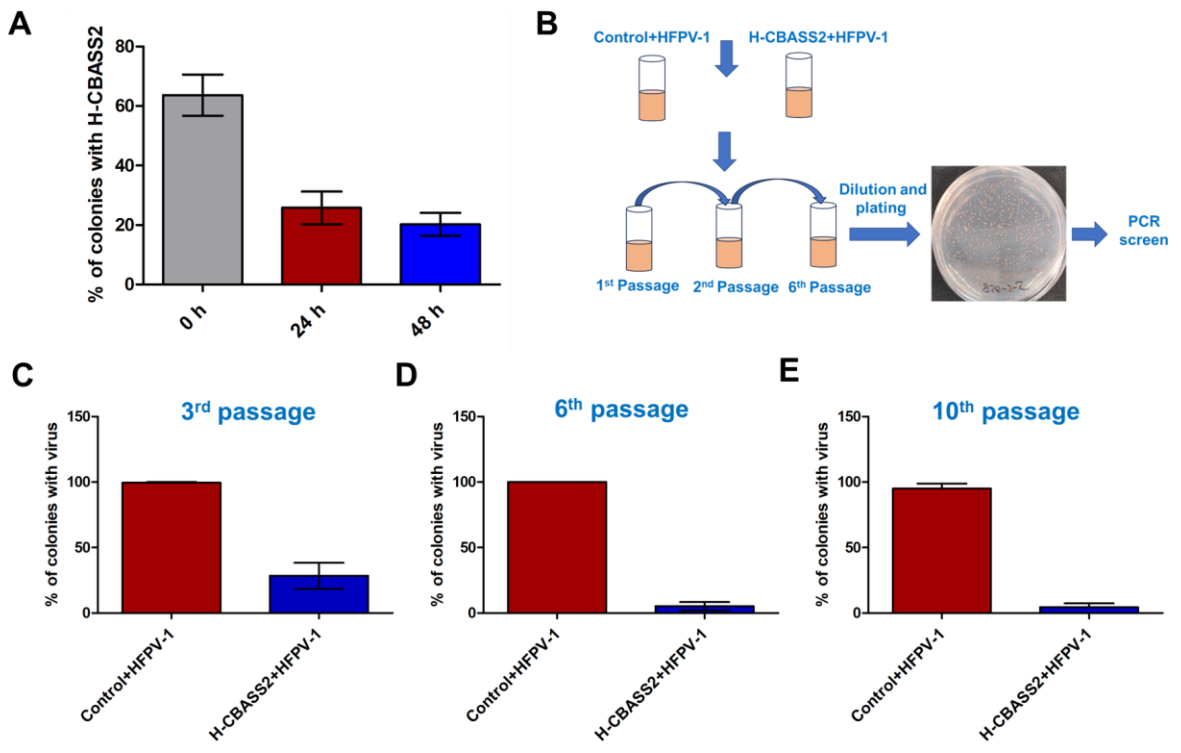

Figure 4. H-CBASS2 clear HFPV-1 infection. A) Head-to-head competition experiments between a virus-infected *H. volcanii* strain carrying the H-CBASS-2 system and a virus-infected control strain lacking that system. Equal amounts of log-phase cultures were mixed into fresh Hv-ECa medium and incubated at 45°C for 48 hours. Samples of 100 µL were taken at 24 and 48 hours and plated on Hv-ECa plates. Once colonies appeared, the presence of CBASS was tested by PCR. Each strain was tested with at least 3 biological replicates. **B)** Schematic representation of an in vitro evolution experiment. In this experiment, a virus-infected *H. volcanii* strain expressing H-CBASS-2 and a control strain infected with the virus were used. Single isolated colonies from each strain (infected with HFPV-1) were inoculated into fresh Hv-ECa medium supplemented with thymidine and tryptophan. The cultures were then serially passaged approximately 10 times in fresh medium. Afterward, the cells were plated on Hv-ECa medium supplemented with thymidine and tryptophan, and the presence of virus DNA was tested by PCR. **C)** Ratio of virus-cured colonies after the 3rd passage. **D)** Ratio of virus-cured colonies after the 6th passage. **E)** Ratio of virus-cured colonies after the 10th passage.

Potential mechanisms underlying virus eradication

Next, we wanted to explore how H-CBASS2-expressing cells eliminate viruses. Recent studies have demonstrated that some defense systems can modify viral proteins and interfere with phage assembly [23] and egress [24]. To test whether H-CBASS2 impairs viral egress from cells, we purified HFPV-1 from the supernatant[13] of both H-CBASS2-expressing cells and control cells after 7 days of continuous growth and conducted plaque assays with these viruses on the same *H. volcani* WR532 reporter strain. We observed that viruses extracted from H-CBASS2-expressing cells were capable of forming plaques as well as the controls (data not shown). Taken together, we conclude that H-CBASS2 is unlikely to directly damage the virus particles.

We then performed proteomic analysis on HFPV-1-infected cells, both with and without H-CBASS2 expression. Of the nine expected viral proteins, we identified six, with several showing substantial differences in abundance between the two conditions (Supplementary Table 1). Most notably, a putative transcriptional regulator was undetectable in protein extracts from H-CBASS2-expressing cells, while the viral spike protein was more than two-fold higher. These findings strongly suggest that H-CBASS2 activity alters the viral lifecycle, which could explain the eradication of the virus from H-CBASS2-expressing cells.

H-CBASS2-containing strains that cleared HFPV-1 infection exhibit improved growth and virus-resistance phenotypes

An additional mechanism that can lead to virus eradication is host evolution of resistance towards that virus. Since we observed that the virus in the supernatant remains active and capable of re-infection, we hypothesized that cells which had cured the virus might develop resistance and outcompete the virus-sensitive population. To test this, we selected four independent colonies that encode H-CBASS2 but had previously been cured of the virus, and performed a plaque assay on colony-derived cells. Surprisingly, we found that all four virus-cured strains exhibited less plaque formation compared to strains derived from the control H-CBASS2-positive colonies that had never been infected with the virus (Fig. 5A).

To identify genomic events that could explain this resistance, we extracted DNA from both H-CBASS2-expressing virus-cured colonies and virus-infected control colonies. We then sequenced the genomes from five colonies of each type obtained at passage 10 to understand what could have mediated viral clearance. Previous research has shown that some defense systems, which induce dormancy rather than cell death, allow CRISPR-Cas sufficient time to acquire spacers from the viral invader's genome, and subsequently, CRISPR-Cas degrades the viral genome. *H. volcanii* has an active CRISPR-Cas system [25–27], yet past work has shown CRISPR-Cas to be unable to clear HFPV-1 infection[13]. Analysis of the CRISPR arrays of the H-CBASS2-expressing clones that cleared the infection showed that no new spacers were acquired, indicating that HFPV-1 eradication probably did not involve CRISPR-Cas activity. Additionally, no mutations in the plasmid from which H-CBASS2 was expressed were detected.

However, we identified several point mutations, some of which occurred in clones derived from more than one colony (Supplementary Table 2). Notably, point mutations in a locus associated with lipoproteins were observed in nearly all virus-cured strains. For example, a single nucleotide deletion - located in the non-coding region upstream of a putative lipoprotein-associated gene (HVO_2285) in *H. volcanii* was shared among 3 out of 5 virus-cured strains.

However, mutations were also detected in the same non-coding region in two CBASS-negative samples, though at different positions. Interestingly, this non-coding region is located within a putative endogenous provirus of *H. volcanii* region known as Halfvol4[28] (Supplementary Table 2)[29]. In addition, we identified a single nucleotide substitution in HVO_2266 an uncharacterized protein also located within a putative endogenous provirus in two control samples. This mutation did not result in any change at the amino acid level. Thus, mutations in this locus probably occur during HFPV-1 infection in both CBASS-positive and CBASS-negative cells, but are more likely to reach fixation in the CBASS-positive.

Additionally, we identified a single nucleotide substitution in another virus-cured strain (which did not have the previously mentioned deletion). This mutation resulted in an amino acid change from valine to alanine in the SRPBCC domain of HVO_1411, which is a domain characterized by a deep hydrophobic ligand binding pocket (citation). In addition, we detected a frameshift mutation in two virus-cured strains in HVO_2141, which encodes a putative lipoprotein.

Interestingly, the virus-cured colonies exhibited a substantial growth advantage compared to both non-infected H-CBASS2-expressing strains and even the empty vector controls (Fig. 5B). Notably, the three fastest-growing strains shared the same mutation in the non-coding region upstream of HVO_2285 described above. Mutations that affect lipoproteins might affect virus entry, which could explain why we observed slight resistance to reinfection. However, the relative contribution of CBASS activity and subsequent mutations to the clearing of the HFPV-1 infection remains unclear.

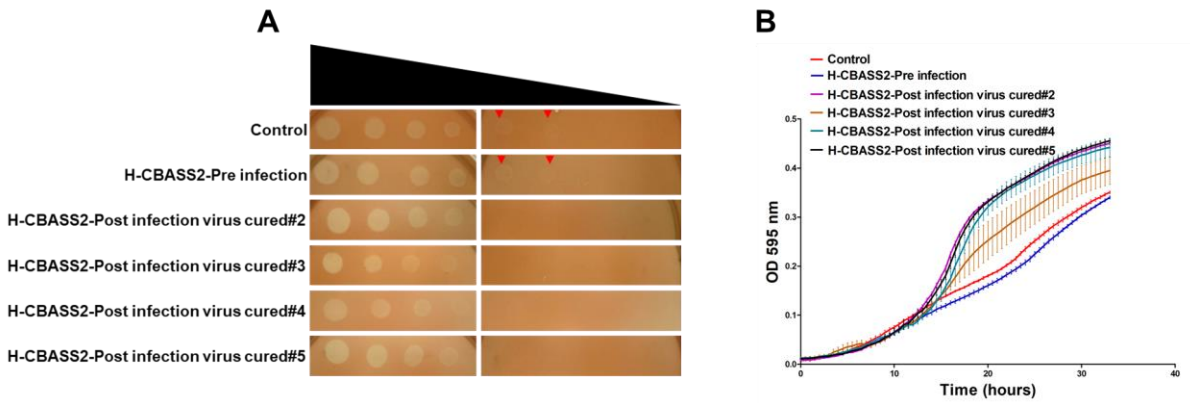

Figure 5. Virus-cured colonies showed resistance to re-infection by HFPV-1. A) Plaquing efficiency of HFPV-1 on different *H. volcanii* strains: H-CBASS2 expressing post-infection virus-cured colonies along with pre-infection (never infected) H-CBASS2 expressing strain and non-infected *H. volcanii* (empty vector) serving as controls. Ten-fold serial dilutions of HFPV-1 were spotted onto the plates (left-most is undiluted, arrow highlighting the plaque). Each strain was tested with at least 3 biological replicates. **B)** Growth curves of individual H-CBASS2 expressing

virus-cured (post-infection) strains. H-CBASS2 expressing strains post-infection from virus-cured colonies #2, 3, 4, and 5 are shown (purple, brown, cyan, and black), along with pre-infection H-CBASS2 expressing strain (blue) and control non-infected strain (red). Lines represent the mean of at least 2 biological replicates, each having three technical replicates.

Conclusion

In this study, we characterize the Type 2 CBASS system fromthe halophilic archaeon *Haloferax* strain Atlit 48N. We observed a significant growth delay upon chronic virus infection, but no cell death occurred during the log phase. Interestingly, when virus-infected H-CBASS2-expressing colonies were left at room temperature for 4–5 weeks, they lost their red pigmentation, and many of them eventually died. Additionally, we did not detect immediate NAD^+ depletion upon virus infection; instead, it only occurred after prolonged incubation at room temperature. These results suggest that depletion of the NAD^+ pool by H-CBASS2 is a slow process in *H. volcanii*, in which oxidative decarboxylation in respiration does not involve the reduction of NAD to NADH, unlike many aerobic bacteria[30], and takes longer to have an effect.

Nonetheless, even during the log phase when NAD^+ levels are normal, growth is delayed, potentially because the cells might already be adjusting their metabolism to conserve NAD^+, which could have a cost. Notably, the growth medium, consisting of casamino acids, does not provide an external source of NAD^+. Taken together, these findings indicate that *H-CBASS2* does not function as a typical abortive infection system during chronic virus infection in *H. volcanii*.

Although we were skeptical about H-CBASS2 being beneficial under chronic virus infection, we nevertheless observed that H-CBASS2-expressing cells cleared HFPV-1 infection: this is probably a combination of a direct effect on HFPV-1, toxicity to the host, which increases the growth advantage of cells that got rid of the virus, and higher resistance of post-infection cells, which is CRISPR-independent.

We found that H-CBASS2 expression interferes with the viral life cycle by altering the expression of specific viral proteins. Furthermore, virus clearance is likely supported by the emergence of host genomic mutations—particularly in lipoprotein-associated genes—which may reduce susceptibility to reinfection. Although the precise contributions of CBASS activity versus host adaptation by mutation remain to be fully understood, our findings highlight a multifactorial mechanism of virus eradication involving both immune signalling and mutation-based adaptation. Our results support the broader view of so-called abortive-infection systems as defenses that often target the virus as well as the host, and can affect infection outcome long before causing cell death[31].

318 **Methods**

319 **Culture conditions-** The Haloferax wild-type strains were routinely cultured at 45°C, either in
320 Hv-YPC or Hv-Ca/Hv-Enhanced Ca medium. *Haloferax volcanii* transformants were selected
321 for and grown either in Hv-Ca or Hv-Enhanced Ca (Hv-ECa). Thymidine 40 µg/ml and
322 tryptophan 50 µg/ml were supplemented when required. Bacterial strains, were cultured at
323 37°C in LB medium or LB medium supplemented with ampicillin for strains carrying plasmids.
324 **Cloning and mutagenesis-** Complete *Haloferax* 48N CBASS Type II system, was cloned into
325 high-copy replicating plasmids pTA927 (which contains the tryptophanase inducible promoter)
326 by using the Gibson assembly method. DNA fragments for the DNA inserts, such as H-
327 CBASS2, and the plasmid vectors were first PCR-amplified with specific primers by using
328 either Phusion or KAPA-HiFi DNA-Polymerase. PCR amplified plasmids and DNA fragments
329 were then purified by the Wizard® SV Gel and PCR Clean-Up kit (Promega) followed by *Dpn*I
330 digestion of purified plasmids. The purified DNA fragments and plasmids were then ligated
331 using the Gibson assembly protocol (Gibson et al., 2009). After ligation, the resulting plasmids
332 were transformed into *E. coli* DH12S cells using the electroporation method. Following the
333 clone confirmation by PCR, the plasmids were extracted using the GenElute™ Plasmid
334 Miniprep Kit from Sigma-Aldrich and transformed into *H. volcanii* strains.
335 **Mutagenesis** -The Cyclase-dead variant of H-CBASS2 cloned into pTA927 was generated by
336 substituting the conserved tyrosine amino acid at position 237 with alanine using site-directed
337 mutagenesis, and the mutation was verified through sequencing.
338 **Transformation with HFPV-1 -** *H. volcanii* strains were grown overnight to the log phase and
339 then harvested by centrifugation at 6,500 rpm for 5 minutes. The pellet was gently
340 resuspended in 200 µl of spheroplasting solution containing 1 M NaCl, 27 mM KCl, 50 mM
341 Tris-HCl, and 15% sucrose. The solution was treated with 0.5 M ethylenediaminetetraacetic
342 acid (EDTA) at pH 8 to chelate any divalent cations present. After incubating for 10 minutes at
343 room temperature, 5-10 µl of concentrated HFPV-1 particles were added to the resuspended
344 culture, followed by another 5-minute incubation at room temperature. After the virus particles
345 were added, 250 µL of 60% PEG600 was gently mixed into the solution. The mixture was then
346 incubated at room temperature for 1 hour. Following the incubation with PEG600, the cells
347 were washed with 1 ml of regeneration solution (Hv-YPC+ media with 15% sucrose). The
348 pellets were then dissolved in Hv-YPC+ media with 15% sucrose and incubated at 28°C for 3
349 hours without shaking. After the 3-hour incubation at 28°C, the cells were transferred to a 28°C
350 incubator shaker for an additional 3 hours. Subsequently, the cells were serially diluted and
351 plated to obtain single colonies. HFPV-1-infected colonies were then identified by PCR using
352 virus-specific primers.

353 **Growth curves-** For all the growth experiments, each strain was grown over-night to the log
354 phase in Hv-ECa medium with thymidine and tryptophan and then diluted into a fresh Hv-ECa
355 medium with thymidine and tryptophan to OD0.03 to 0.05 and further kept at 42°C for 72 h
356 with continuous shaking in 96-well plates. For induction, L-tryptophan (Sigma Aldrich) was
357 added to the diluted culture to achieve a final concentration of 2 mM. Turbidity of the culture
358 (OD595nm) was measured every 30 minutes using a microplate reader (Biotek ELX808IU-
359 PC). For each strain, we performed a minimum of three biological replicates, with each
360 biological replicate comprising three technical replicates.
361 **Live/Dead staining-** To evaluate the viability of virus-infected *H. volcanii* strains expressing
362 H-CBASS-2, we conducted a Live/Dead staining experiment using the LIVE/DEAD BacLight
363 Bacterial Viability Kit from Thermo-Fisher (Ref-L13152). To determine the ratio of dead cells
364 from the logarithmic phase culture, each strain was grown overnight. The cultures were then
365 diluted into fresh medium to an optical density (OD) of 0.03 to 0.05 and incubated in a 45°C
366 shaking incubator until they reached the logarithmic phase. Following that, 100 µl of the
367 resuspended cultures were aliquoted into 1 ml Eppendorf tubes for subsequent analysis. Next,
368 10 µl of Propidium iodide dye and 10 µl of SYTO9 dye were added separately from their
369 respective stock solutions. The treated cultures were then incubated in the dark for 15-20
370 minutes to allow for the cellular uptake of the stains. After the incubation period, 10 µl of the
371 treated culture were placed onto a glass slide and examined using a confocal microscope
372 (Leica sp8 confocal microscope) at magnifications of 20x and 40x. To evaluate dead cells from
373 the bleached colonies, cells were directly taken from the plates showing bleached colonies
374 and mixed into 100 µl of Hv-ECa medium. Subsequently, the mixed cells were washed twice
375 with Hv-ECa medium and then subjected to the aforementioned microscopy protocol.
376 **Plate colony pigmentation assays-** For these plate assays, each strain was grown overnight
377 to the log phase and then diluted to a fresh medium to OD 0.05, 20 µl of sample streaked on
378 the new plates and kept at 45°C for 4-5 days. After the cells grew, all the plates were left at
379 room temperature for 4-6 weeks, and images were captured every three days.
380 **NADase assay-** Total cellular NAD level was measured using the NAD/NADH Quantification
381 Kit from Sigma-Aldrich (MAK037). Each strain was grown to the late log phase, and then a
382 roughly equal number of cells was taken from each culture, estimated by optical density. The
383 cells were washed twice with cold Hv-Ca media. The pelleted cells for each assay were
384 transferred to a 1.5 ml microcentrifuge tube and centrifuged at 3000 rpm for 5 minutes. The
385 resulting cell pellet was then resuspended in 400 µl of NADH/NAD extracted buffer. The cells
386 were lysed by subjecting them to two rounds of sonication. After sonication, the cells were
387 centrifuged at 13,000 rpm for 10 minutes, and the supernatant was transferred to a different
388 microcentrifuge tube. The samples were then deproteinized using Amicon 10 kDa cut-off spin
389 filters by centrifugation. Subsequently, 50 µl of deproteinized extracted sample from each

replicate was transferred into 96-well plates. Into each well, 100 µl of master reaction mixture (comprising 98 µl of NAD cycling buffer and 2 µl of NAD cycling enzyme mix) was added. The plates were then incubated at room temperature for 5 minutes. After the 5-minute incubation with the master reaction mixture, 10 µl of NADH Developer was added to each well. The plates were then incubated at room temperature for 1 to 2 hours. Absorbance at 450 nm was measured to assess the reaction. To measure the NAD level from the bleached cells, cells were directly taken from the bleached plates and mixed into 1 ml of cold Hv-Ca media. The cells were then washed twice. As previously described, the cells for each assay were pelleted in a 1.5 ml microcentrifuge tube at 3000 rpm for 5 minutes. The pellet was then resuspended in 400 µl of NADH/NAD extracted buffer, and the cells were lysed by two rounds of sonication. After sonication, the protein concentration was measured using the Bradford assay. The NAD assay protocol was then followed as described previously

Long-term growth experiments- Single isolated colonies from each strain (*H. volcanii* strain with H-CBASS-2 and a control strain infected with the virus) were inoculated into a liquid culture contains Hv-ECa +Thymidine and tryptophan until the late log or stationary phase and then used the culture to inoculate fresh medium and so forth for ~10 passages. Following 10 passages 100 ul of culture from each sample were serially diluted in fresh Hv-Ca medium and plated on Hv-Ca +Thymidine and tryptophan plates. 30-40 colonies were screened by PCR do determine the presence of HFPV-1 virus in each sample.

Plaque Assay- For the plaque assay, *H. volcanii* strains were grown overnight in Hv-ECa medium and normalized at optical density of 595 nm (OD595). Subsequently, 400 µl of cultures with 0.5M CaCl2 was added to 3-4 ml of 0.2% top-agar (preheated and cooled to 60°C) in Hv-YPC, and the mixture was spread onto rich agar plates with 18% SW. Next, incubated at room temperature for 15 to 20 minutes, a ten-fold serial dilution of HFPV-1 was made into Hv-ECa, and 3 ul of different dilution were spotted. After 2 days of incubation at 30°C, plaques were formed. Afterward, the plates were left on the bench at around 25°C for 2-3 days, during which time the plaques continued to grow and become more distinct. Images were captured to document the growth and appearance of the plaques.

Quantitative real-time PCR (Q-PCR)- To quantify the genome, copy number (gcn) of *H. volcanii* and HFPV-1, we used the CFX Connect Real-Time PCR system (Bio-Rad Laboratories). We collected 1 ml of cultures in biological triplicates at 48 and 72 hours, as well as during the 3rd and 6th passages. These cultures were pelleted at 11,000 × g for 10 minutes at room temperature and supernatant was collected. To assess the amount of secreted viral DNA in the supernatant, DNA was extracted from 200 µl of the supernatant using the Quick-DNA Viral Kit (Zymo Research, D3015). Quantitative PCR (qPCR) was performed using the q-PCRBIO SyGreen Blue mastermix Hi-ROX (Cat. No- PB20.16-05) with primers specific to

an internal viral protein and a housekeeping gene, the DNA polymerase II small subunit (*polB*). The cycle threshold (CT) values of viral DNA were normalized to the respective CT values of *polB*.

Competition assay- To perform head-to-head competition experiments, we used a virus-infected *H. volcanii* strain carrying the H-CBASS-2 system and a virus-infected control strain lacking this system. Each strain was grown overnight to the log phase in Hv-ECa medium supplemented with thymidine and tryptophan. Equal amounts of the log-phase cultures (OD 0.03) were then mixed into fresh Hv-ECa medium and incubated at 45°C for 48 hours with continuous shaking. Samples of 100 µL were taken at 0, 24, and 48 hours, diluted, and plated on Hv-ECa plates containing thymidine and tryptophan. After colonies appeared, the presence of the CBASS gene cluster was verified using internal specific primers for H-CBASS2 by PCR.

New mutation detection- To check for new mutations and CRISPR spacer acquisition, we selected three individual colonies from each post-infection virus-cured *H-CBASS2*-expressing strain, as well as from the virus-infected wild-type strain after the 10th passage. DNA was extracted using the Blood and Tissue Kit (Qiagen, 69506). Whole genome sequencing was performed by Plasmidsaurus. using Oxford Nanopore Technology with custom analysis and annotation. Mutations in the main chromosome were identified by comparing the main chromsome obtained from each colony to DS2 *H. volcanii* reference genome, using MUMmer 3.0 with default parameters.

Homology modelling using AlphaFold3- To create a homology model of the H-CBASS2 cyclase, we employed a multi-step process based on AlphaFold3 structure prediction[32]. We first extracted the amino acid sequence of the H-CBASS2 cyclase (accession number: WP_115891644.1) from the NCBI database. The extracted sequence was submitted to the AlphaFold3 server for predicted strcuture generation. After obtaining the model, we conducted a Foldseek[33] search for structural comparison against the PDB database. The resulting structure was analyzed based on TM-score and RMSD (Root Mean Square Deviation) values. Finally, we used the UCSF Chimera software to visualize the alignments and generate the figures.

Proteomics- For proteomic analysis, we used a virus-infected *H. volcanii* strain carrying the H-CBASS-2 system and a virus-infected control strain lacking this system. Each strain was grown to the late log phase in Hv-ECa medium. The cultures were centrifuged at 4,500 × g for 45 minutes to collect the cell pellet. The supernatant was collected, and the viruses were precipitated by adding polyethylene glycol (PEG) 6000 to a final concentration of 10% (wt/vol), followed by incubation at 4°C overnight. After overnight incubation, viruses were extracted according to the protocol described by Tomas Alarcon-Schumacher et al. [13]. The cell pellet

461 and extracted viral particles were sent directly to the Smoler Proteomics Center at the Lorry I.
462 Lokey Interdisciplinary Center for Life Sciences and Engineering, Technion, Israel. The
463 samples were digested with trypsin and analyzed by LC-MS/MS using the Q Exactive HFX
464 mass spectrometer. Data analysis was performed using Proteome Discoverer 2.4 software
465 and the Sequest search engine against both a specific database and a decoy database to
466 determine the false discovery rate (FDR). All identified peptides were filtered with a high-
467 confidence 1% FDR threshold. Quantification was carried out by calculating the peak area of
468 each peptide, with protein abundance represented by the sum of all associated peptide group
469 abundances.

470 **Author contributions**

471 U.G. and D.K.C. conceived and designed the study. D.K.C. performed the experiments. H.S.,
472 D.K.C., N.G., D.V., and L.R. analyzed the data. D.K.C. prepared the figures and analyzed the
473 data with input from U.G. The manuscript was written by D.K.C., with U.G. and L.R.
474 contributing to its editing. All authors read and approved the final draft.

475 **Acknowledgements**

476 The authors thank Prof. Susanne Erdmann for providing HFPV-1, Sharon Navok for
477 assistance with the development and execution of plaque assays, and Alex Barbul for help
478 with confocal microscopy. The authors also thank Dr. Israela Turgeman-Grott and Neta
479 Altman-Price for helpful discussions. The work is dedicated to the memory of Rachel
480 Schreiber.

481

482 **Funding**

483 This research was supported by the European Research Council (grant ERC- AdG 787514),
484 and the Israeli Science Foundation (grant 1599/24). The funding agencies had no involvement
485 in the study design, data collection, analysis, or interpretation, in the writing of the manuscript,
486 or in the decision to publish the findings.

487 **Conflict of interest**

488 The authors declare that they have no conflict of interest.

489 **References**

490 1. Cohen, D. *et al.* Cyclic GMP–AMP signalling protects bacteria against viral infection.
491 *Nature* **574**, 691–695 (2019).

492 2. Lowey, B. *et al.* CBASS Immunity Uses CARF-Related Effectors to Sense 3'-5'- and
493 2'-5'-Linked Cyclic Oligonucleotide Signals and Protect Bacteria from Phage Infection. *Cell*
494 **182**, 38-49.e17 (2020).

3. Ofir, G. *et al.* Antiviral activity of bacterial TIR domains via immune signalling molecules. *Nature* **600**, 116–120 (2021).

4. Duncan-Lowey, B., McNamara-Bordewick, N. K., Tal, N., Sorek, R. & Kranzusch, P. J. Effector-mediated membrane disruption controls cell death in CBASS antiphage defense. *Mol. Cell* **81**, 5039-5051.e5 (2021).

5. Tesson, F. *et al.* Systematic and quantitative view of the antiviral arsenal of prokaryotes. *Nat. Commun.* **13**, 2561 (2022).

6. Rousset, F. *et al.* A conserved family of immune effectors cleaves cellular ATP upon viral infection. *Cell* **186**, 3619-3631.e13 (2023).

7. Wein, T. & Sorek, R. Bacterial origins of human cell-autonomous innate immune mechanisms. *Nat. Rev. Immunol.* **22**, 629–638 (2022).

8. Whiteley, A. T. *et al.* Bacterial cGAS-like enzymes synthesize diverse nucleotide signals. *Nature* **567**, 194–199 (2019).

9. Morehouse, B. R. *et al.* STING cyclic dinucleotide sensing originated in bacteria. *Nature* **586**, 429–433 (2020).

10. Millman, A., Melamed, S., Amitai, G. & Sorek, R. Diversity and classification of cyclic-oligonucleotide-based anti-phage signalling systems. *Nat. Microbiol.* **5**, 1608–1615 (2020).

11. Hogrel, G. *et al.* Cyclic nucleotide-induced helical structure activates a TIR immune effector. *Nature* **608**, 808–812 (2022).

12. Morehouse, B. R. *et al.* Cryo-EM structure of an active bacterial TIR–STING filament complex. *Nature* **608**, 803–807 (2022).

13. Alarcón-Schumacher, T., Naor, A., Gophna, U. & Erdmann, S. Isolation of a virus causing a chronic infection in the archaeal model organism Haloferax volcanii reveals antiviral activities of a provirus. *Proc. Natl. Acad. Sci. U. S. A.* **119**, e2205037119 (2022).

14. Govande, A. A., Duncan-Lowey, B., Eaglesham, J. B., Whiteley, A. T. & Kranzusch, P. J. Molecular basis of CD-NTase nucleotide selection in CBASS anti-phage defense. *Cell Rep.* **35**, 109206 (2021).

15. Navok, S., Cohen, L., Ron, E. Z. & Gophna, U. Optimized Plaque Assay for Detecting Chronically Infecting Viruses of Haloarchaea. 2024.11.12.619373 Preprint at https://doi.org/10.1101/2024.11.12.619373 (2024).

16. Green, M. R. & Sambrook, J. Plating Bacteriophage M13. *Cold Spring Harb. Protoc.* **2017**, pdb.prot093427 (2017).

17. Giani, M., Miralles-Robledillo, J. M., Peiró, G., Pire, C. & Martínez-Espinosa, R. M. Deciphering Pathways for Carotenogenesis in Haloarchaea. *Mol. Basel Switz.* **25**, 1197 (2020).

18. Kellermann, M. Y., Yoshinaga, M. Y., Valentine, R. C., Wörmer, L. & Valentine, D. L. Important roles for membrane lipids in haloarchaeal bioenergetics. *Biochim. Biophys. Acta BBA - Biomembr.* **1858**, 2940–2956 (2016).

19. Vögeli, B. *et al.* Archaeal acetoacetyl-CoA thiolase/HMG-CoA synthase complex channels the intermediate via a fused CoA-binding site. *Proc. Natl. Acad. Sci.* **115**, 3380–3385 (2018).

20. Makarova, K. S., Anantharaman, V., Aravind, L. & Koonin, E. V. Live virus-free or die: coupling of antivirus immunity and programmed suicide or dormancy in prokaryotes. *Biol. Direct* **7**, 40 (2012).

21. Williams, M. C. *et al.* Restriction endonuclease cleavage of phage DNA enables resuscitation from Cas13-induced bacterial dormancy. *Nat. Microbiol.* **8**, 400–409 (2023).

22. Meeske, A. J., Nakandakari-Higa, S. & Marraffini, L. A. Cas13-induced cellular dormancy prevents the rise of CRISPR-resistant bacteriophage. *Nature* **570**, 241–245 (2019).

23. Millman, A. *et al.* An expanded arsenal of immune systems that protect bacteria from phages. *Cell Host Microbe* **30**, 1556-1569.e5 (2022).

24. Hör, J., Wolf, S. G. & Sorek, R. Bacteria conjugate ubiquitin-like proteins to interfere with phage assembly. *Nature* **631**, 850–856 (2024).

25. Stachler, A.-E. *et al.* High tolerance to self-targeting of the genome by the endogenous CRISPR-Cas system in an archaeon. *Nucleic Acids Res.* **45**, 5208–5216 (2017).

26. Maier, L.-K. *et al.* The nuts and bolts of the Haloferax CRISPR-Cas system I-B. *RNA Biol.* **16**, 469–480 (2018).

27. Turgeman-Grott, I. *et al.* Pervasive acquisition of CRISPR memory driven by inter-species mating of archaea can limit gene transfer and influence speciation. *Nat. Microbiol.* **4**, 177–186 (2019).

28. Cianni, N. D. *et al.* Provirus deletion from Haloferax volcanii affects motility, stress resistance and CRISPR RNA expression. 2024.10.11.617810 Preprint at https://doi.org/10.1101/2024.10.11.617810 (2024).

29. Hayes-Smith, C. N. Genetic analysis of radiation resistance in Haloferax volcanii.

30. Pfeiffer, F. & Dyall-Smith, M. Open Issues for Protein Function Assignment in Haloferax volcanii and Other Halophilic Archaea. *Genes* **12**, 963 (2021).

31. Aframian, N. & Eldar, A. Abortive infection antiphage defense systems: separating mechanism and phenotype. *Trends Microbiol.* **31**, 1003–1012 (2023).

32. Abramson, J. *et al.* Accurate structure prediction of biomolecular interactions with AlphaFold 3. *Nature* **630**, 493–500 (2024).

33. van Kempen, M. *et al.* Fast and accurate protein structure search with Foldseek. *Nat. Biotechnol.* **42**, 243–246 (2024).